"Snubbers For Limiting And Mitigating Fault Energy During The Accelerator Grid Breakdown For DNBPS"

Major Project Report

Submitted in Partial Fulfillment of the Requirements for

Degree of

MASTER OF TECHNOLOGY

IN

ELECTRICAL ENGINEERING

(Electrical Power System)

by

Palak P. Patel

(11MEEE19)

Department of Electrical Engineering

INSTITUTE OF TECHNOLOGY

NIRMA UNIVERSITY

AHMEDABAD 382 481

May 2013

CERTIFICATE

This is to certify that the Major Project Report entitled **"Snubbers For Limiting And Mitigating Fault Energy During The Accelerator Grid Breakdown For DNBPS"** submitted by **Ms. Palak P. Patel (11MEEE19)** towards the partial fulfillment of the requirement for the award of degree in Master of Technology (Electrical Engineering) in the field of Electrical Power System of Nirma University is the record of work carried out by her under our supervision and guidance. The work submitted has in our opinion reached a level required for being accepted for examination. The results embodied in this major project work to the best of our knowledge have not been submitted to any other University or Institution for award of any degree or diploma.

Date: / /

Industry Guide:
Mr. N. P. Singh
Engineer-SE, Power Supply Group
ITER-India
(Institute For Plasma Research)
Gandhingar 382025.

Date: / /

Institute Guide:
Prof. S.N. Jani
Assistance Professor
Department of Electrical Engineering.
Nirma University
Ahmedabad 382481.

Head of Department:
Department of Electrical Engineering
Institute of Technology
Nirma University
Ahmedabad

Director:
Institute of Technology
Nirma University
Ahmedabad

Acknowledgements

With immense pleasure, I would like to present this report on the dissertation work related to 'Snubbers For Limiting And Mitigating Fault Energy During The Accelerator Grid Breakdown For DNBPS'. I am very thankful to all those who helped me for the successful completion of the first phase of the dissertation and for providing valuable guidance throughout the project work.

I would first of all like to offer thanks to **Mr. N. P. Singh**,(ITER-India,IPR) Industry Project Guide whose keen interest and excellent knowledge base helped me to finalize the topic of the dissertation work. His constant support, encouragement, and constructive criticism has been invaluable assets through my project work. He has shown keen interest in this dissertation work right from beginning and has been a great motivating factor in outlining the flow of my work.

I am also very thankful to my institute guide **Prof. S. N. Jani** who helped me in every difficulty in project work and every thing related to the project.

I would like to thank **Mr. Amit Patel** & **Mr. Kapil Oza** (ITER-India,IPR) co-operated me for my project work.

Finally, I would like to thank The Almighty, my family members for supporting and encouraging me in all possible ways. They have provided continuous encouragement in making this dissertation work successful.

- Palak P.Patel

11MEEE19

Abstract

The ITER DNB system is based on the acceleration of negative ions; designed to inject 60A of Neutral beam at (-) 100kV with specified modulation in to the plasma. The acceleration grids operate very close to breakdown. During conditioning and normal operation of the injector, breakdowns can occur frequently and unpredictably. It is important to limit as much as possible the energy flowing into the grids. This energy comes from the power supplies and from the electrostatic energy stored in the transmission line and stray capacitances. Core snubbers (annular disc of magnetic material) are considered to be most promising options for limiting the fault energy during the breakdowns in the accelerators. This report presents the study and overview of DNBPS system, design approach for the snubbers- circuit model, simplified model of the grid break down circuit, effect of snubber impedance on the short circuit current. As a prerequisite, simulation software (Pspice) been exposed to have hands-on experience. An experimental setup is been used to study and characterize the actual size CRGO core snubber. Results are discussed to investigate the feasibility of CRGO cores. In order to assess the effectiveness of snubbers, a refined model having frequency dependency should be developed. The model should be able to take in to account the presence of DC component. Reported work presents the development of refined snubber model using PSIM tool.

List of Figures

List of Tables

Abbreviations

AC ... Alternating Current
ACCPS ... Active Correction Coil Power Supply
AGPS ... Accelerator Grid Power Supply
BPS ... Bias Power Supply
CRGO ... Cold rolled Grain Oriented
DC ... Direct Current
DNB ... Diagnostic Neutral Beam
DNBPS ... Diagnostic Neutral Beam Power Supply
EGPS ... Extraction Grid Power Supply
GRPS ... Ground Related Power Supply
HV ... High Voltage
HVCC ... High Voltage Coaxial Cable
HVD ... High Voltage Deck
ID ... Inner Diameter
ISEPS ... Ion Source and Extractor Power Supplies
ITER ... International Thermonuclear Experimental Reactor
OD ... Outer Diameter
PGFPS ... Plasma Grid Filter Power Supply
PSIM ... Power Sim
RF ... Radio Frequency
RFPS ... Radio Frequency Power Supply
RID ... Residual Ion Dump
RIDPS ... Residual Ion Dump Power Supply
s.m.m. ... Soft Magnetic Materials
TL ... Transmission Line

Nomenclature

A_e .... Effective area of the toroid core
AL .... Inductance Factor
B .... Magnetic induction = Magnetic flux density
B_{Peak} .... Peak flux density in the core
B_{sat} .... Saturation flux density in the core
C .... Capacitance of the coaxial Cable
C_1 .... Toroidal core constant 1
C_2 .... Toroidal core constant 2
E .... Energy
E_c .... Energy dissipated by the core
$E_{deconditioning}$ .... Deconditioning Energy
E_f .... Energy dumped in the fault
E_{stored} .... Stored Energy in the coaxial TL
f .... frequency
H .... Magnetic field
H_2 .... Hydrogen Molecule
h .... Height of the core
I .... Current
I_m .... Maximum current from Inductor winding
I_{sat} .... Saturation current
i_1 .... Eddy current
i_2 .... Load current
K_1 .... Coefficient K_1 for core B-H curve
K_2 .... Coefficient K_2 for core B-H curve
K_{exp1} .... Coefficient K_{exp1} for core B-H curve
K_{exp2} .... Coefficient K_{exp2} for core B-H curve
L_0 .... Inductance considered with unit relative permeability
L_c .... Inductance of the core
L_{DC} .... DC core inductivity
L_m .... Mean Length of the Core
L_P .... Parallel inductance
L_S .... Series inductance
N .... Number of turns
P_{loss} .... power loss
R .... Resistance
R_c .... Resistance of the core
R_f .... Resistance of the fault
R_L .... Resistance of the load
R_P .... Parallel resistance
R_S .... Series resistance
r_1 .... Inner radius of the core

r_2 .... Outer radius of the core
r_{avg} .... Average radius of the core
t .... Time
$tan\delta$ .... loss tangent
V .... Supply Voltage
V_m .... Maximum Voltage across Inductor winding
X_L .... Inductive Reactance
Z .... Impedance of the winding
Δt .... time delay
δ .... Phase delay of B from H
ε_0 .... Absolute permittivity
ε_r .... Relative permittivity
θ .... Impedance Angle
μ .... Permeability
μ_0 .... Absolute Permeability
μ' .... Real Permeability
μ'' .... Imaginary Permeability
μ'_P .... Real component of the complex permeability for parallel representation
μ''_P ... Imaginary component of the complex permeability for parallel representation
μ_r .... Relative Permeability
μ'_S .... Real component of the complex permeability for series representation
μ''_S ..... Imaginary component of the complex permeability for series representation
ρ .... Resistivity
ϕ .... Phase angle
ϕ .... Flux linked in the core
ϕ_{sat} .... Saturation flux in the core

Suffixes

0 .... Absolute component
c .... Core
DC .... Direct Current
f .... Fault condition component
L .... Load component
P .... Parallel element
r .... Relative component
S .... Series element
sat .... saturation condition

Constants

$e = 2.71828$
$j = \sqrt{-1}$
$\mu_0 = 4\pi \times 10^{-7}$ H/m
$\pi = 3.14159$
$\varepsilon_0 = 8.854 \times 10^{-12} F/m$

Contents

1

Introduction

The ITER DNB system is based on the acceleration of negative ions; designed to inject 60A of Neutral beam at (-) 100kV with specified modulation in to the plasma. Diagnostic Neutral Beam (DNB) Injector System of ITER is based on the extraction/acceleration of negative Ions produced by the beam source which consists of RF ion source for Plasma formation, where the negative ions are produced. An extractor, which extracts the ions from the source, and an accelerator which accelerates the extracted negative ions up to 100 keV. The ion source will be at the appropriate high negative potential and the ions are accelerated to ground potential. Partial neutralization of the accelerated negative ion beam is achieved by collisions between the negative ions and H_2 in the neutraliser.The charged fractions of the beam emerging from the neutraliser are removed from the H^0 beam path in a controlled manner by the residual ion dump (RID).To remove the positive and negative beam fractions, an electrical field is applied between the panels making up the RID. The block diagram is as shown in Fig. 1.1.

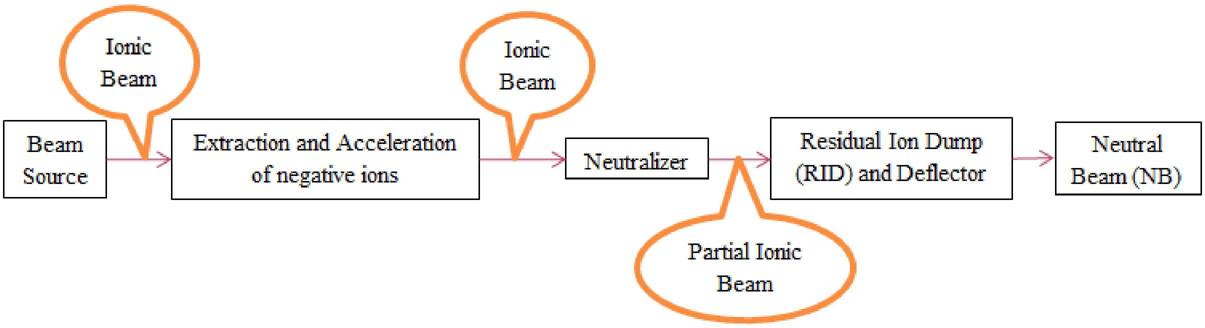

Figure 1.1: Principle of the Neutral Beam Injection System

Maximum beam energy	100 keV
Energy range	40 to 100 keV
Accelerated beam current at maximum energy	60 A

Table 1.1: Performance specification of the ITER DNB source

Table 1.1 shows some performance spacifications of the ITER DNB source

1.1 Functional description of the DNB Power Supply System

The DNB power supply system is described in five different groups of equipment as below:

a. The acceleration grid power supply (AGPS) provides a negative voltage (up to 100kV to ground) to the beam source for acceleration of negative ions. (Up to 8MW)

b. The ion source and extractor power supplies (ISEPS) provide different voltages and current (either in DC or in AC) to several equipment at -100kV reference potential to ground. (Up to 5MW).

Plasma formation and extraction of negative ions is achieved by ISEPS. The ISEPS is composed of four independent equipment:

- RF generator (RFPS), for Plasma formation
- Extraction Grid (EGPS),for extraction of negative Ions
- Bias (BPS) and Plasma Grid Filter (PGFPS) power supplies, for negative Ion enhancement

The voltage rating of these power supplies ranges between some volts to about 12 kV.

c. High Voltage Deck and Transmission Line, for transport of ISEPS and AGPS power to the Beam source.

d. A third group of power supplies called ground related power supplies (GRPS). (Up to 1.8MW) Removal of charged fraction of the beam after neutralizer and field compensation/correction by GRPS, GRPS consists of:

- Residual Ion Dump Power Supply (RIDPS)
- Active Correction Coil Power Supply (ACCPS)

e. DNB Plant control System.

1.2 Block Diagram of DNBPS system

The DNBPS System provides the electrical power at High Voltage to the accelerator grids and supplies the ion source and the auxiliary components. A simplified block scheme of the DNB PS system is shown in Figure 1.2.
The section supplying the acceleration grids is called Acceleration Grid Power Supply (AGPS).

The section inside an air-insulated deck box called High Voltage Deck 1 (HVD1)

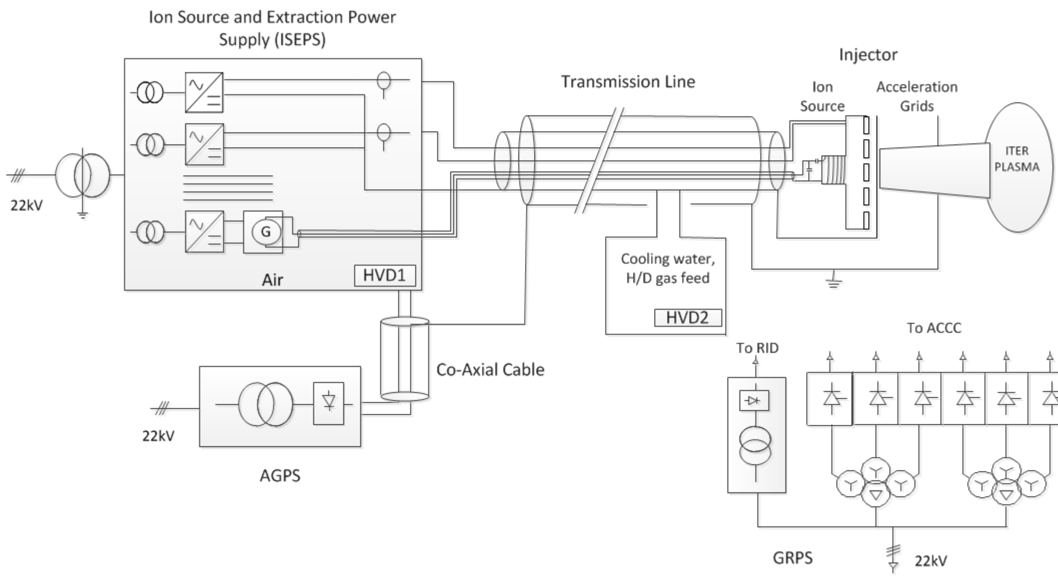

Figure 1.2: Block Diagram of DNBPS system

contains the equipment making up the ISEPS. The ISEPS supplies all the electrical power required by the ion source. All the power supply equipment installed in HVD1 at -100kV to ground are fed by one 50 Hz insulating transformer. This deck can be easily accessed once the system is de-energized.

Another section of the DNBPS system is the Ground Related Power Supplies (GRPS). GRPS is referred to ground and include the power supply systems to feed the Residual Ion Dump (RID) and ITER magnetic field compensation coils i.e. ACCC.

The power is transmitted to the ion source and the acceleration grids via high voltage coaxial cable (HVCC) from AGPS to HVD1 and a high voltage air insulated transmission line (TL) from HVD1 to DNB ion source. Through the internal duct of the TL, cables and conductors of AGPS, ISEPS, cooling water lines, instrumentation cables are carried to the ion source.*Last part of the TL contains the energy limiting snubbers.*

The box called HVD2 contains the, equipment for cooling water, gas feed and if required electronics related to Ion source.

2

Formation of the Problem

The accelerator consists of two metallic grids, called the extraction grid and earth grid. Each grid is divided into segments, each with multiple apertures. Negative ions after the extraction, enter the acceleration region and get accelerated to the desired high energy -100keV.

2.1 Accelerator grid breakdown

Due to micro-protrusion on the edges of the acceleration grids they operate close to breakdown. During conditioning and normal operation of the injector, breakdowns can occur frequently and unpredictably.

Therefore the breakdown cannot be considered as a fault even if it can cause stresses on the HV circuits and power supplies. To minimize the consequences, the DNB system shall sustain this condition repetitively without any damage to power supply or ion source. In addition, the power supply system shall be able to restart operation as soon as possible to minimize loss of diagnostic signals.

Whenever a breakdown occurs, the electric potential of the grids falls to zero very quickly and all the energy stored upstream is discharged in the fault and circuit elements. It is important to limit the energy dumped on the accelerator grigs below the deconditioning limit (20J), beyond that it can cause irreversible damage to the grids. This energy comes from the power supplies and from the electrostatic energy stored in the HV cable/transmission line and in the HVDs stray capacitances, in the Ion Source and HV bushing stray capacitances.

The energy coming from the discharge of the stray capacitances placed upstream of the Ion Source can be limited by inserting passive elements in different part of the HV circuit, e.g. core snubbers, series resistors, dumper circuits, varistors.

The energy coming from the power supply system can be limited by switching off as fast as possible the accelerator and extractor grid power supplies. After a breakdown the AGPS shall be able to reapply in about 20 ms.

Key words: Energy limitation, reapplication

For example:-

Find whether the stored energy in the coaxial cable (having the outer diameter = 1200 mm, inner diameter = 650 mm and length=130m) charged at 100 kV , exceeds the deconditioning limit say 20 J.

Solution:-

From coaxial system , We know that,

$$C = \frac{2\pi\varepsilon_r\varepsilon_0}{\ln(b/a)} \quad (2.1)$$

where,

C = capacitance of the coaxial cable

ε_r = relative permittivity = 1 for air

ε_0 = absolute permittivity = $8.854 \times 10^{-12}\ F/m$

b = outer diameter of the cable

a = inner diameter of the cable

now from eq.(2.1)

$$
\begin{aligned}
C &= \tfrac{2\pi\varepsilon_r\varepsilon_0}{ln(b/a)} \\
&= \tfrac{2\times3.14\times1\times8.854\times10^{-12}}{ln(1200/600)} \\
&= \tfrac{55.578\times10^{-12}}{ln(1.8462)} \\
&= \tfrac{55.578\times10^{-12}}{0.61313} \\
&= 90.6464\ nF/m
\end{aligned}
$$

we know that,

$$E = \frac{1}{2}CV^2 \tag{2.2}$$

$$
\begin{aligned}
E &= \tfrac{1}{2}\times 90.646\times 10^{-12}\times(100\times10^3)^2 \\
&= 45.3232\times10^{-2} \\
&= 0.453232\ J/m
\end{aligned}
$$

$$
\begin{aligned}
E_{stored} &= 0.453232\times130 \qquad (\because\ here\ length\ is\ 130m) \\
&= 58.92J \approx\ 59\ J
\end{aligned}
$$

$$E_{stored} > E_{deconditioning} \tag{2.3}$$

Therefore,it can be said from the eq. (2.3), that the energy stored in the transmission line is too high than the deconditioning limit. This clearly advocates the deployment of the snubbers.

3

Snubber Representation

Snubber as annular magnetic disc(where current carrying current passing through it)can be electrically represented as parallel R and L. Where R represents the loss component and L represents the inductive element.

Basic circuit analysis is performed connecting the snubber in line with the fixed load R_L and a voltage source V

The behavior of the load current is studied for variation of R_c and L_c.(fig. 3.1)

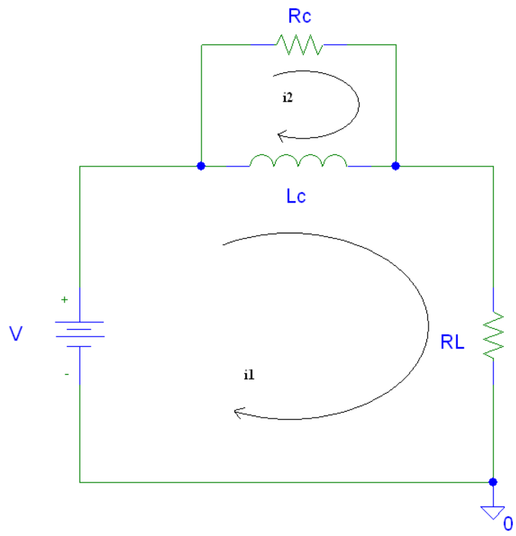

Figure 3.1: Basic Circuit Diagram

$$
\begin{aligned}
V &= L_c \tfrac{d}{dt}(i_1 - i_2) + R_L i_1 & (3.1)\\
V - R_L i_1 &= L_c \tfrac{di_1}{dt} - L_c \tfrac{di_2}{dt} \\
L_c \tfrac{di_1}{dt} &= L_c \tfrac{di_2}{dt} - R_L i_1 + V & (3.2)\\
0 &= L_c \tfrac{d}{dt}(i_2 - i_1) + R_c i_2 & (3.3)\\
L_c \tfrac{di_2}{dt} - L_c \tfrac{di_1}{dt} &= -R_c i_2 \\
L_c \tfrac{di_1}{dt} &= L_c \tfrac{di_2}{dt} + R_c i_2 & (3.4)
\end{aligned}
$$

from eq. (3.2) and (3.4),

$$
\begin{aligned}
L_c \tfrac{di_2}{dt} - R_L i_1 + V &= L_c \tfrac{di_2}{dt} + R_c i_2 \\
R_c i_2 + R_L i_1 &= V & (3.5)
\end{aligned}
$$

from eq. ((3.5)),

$$
\begin{aligned}
i_1 &= \frac{V - R_c i_2}{R_L} & (3.6)\\
i_2 &= \frac{V - R_L i_1}{R_c} & (3.7)
\end{aligned}
$$

put eq. (3.6) in (3.2),

$$
\begin{aligned}
L_c \tfrac{d}{dt}(\tfrac{V-R_c i_2}{R_L}) &= L_c \tfrac{di_2}{dt} - R_L(\tfrac{V-R_c i_2}{R_L}) + V \\
\tfrac{L_c V}{R_L} - \tfrac{L_c R_c}{R_L}\tfrac{di_2}{dt} + V - R_c i_2 - L_c \tfrac{di_2}{dt} &= V \\
\tfrac{L_c V}{R_L} - R_c i_2 - L_c(\tfrac{R_c}{R_L}+1)\tfrac{di_2}{dt} &= 0 \\
L_c(\tfrac{R_c}{R_L}+1)\tfrac{di_2}{dt} + R_c i_2 &= \tfrac{L_c V}{R_L} \\
\tfrac{L_c}{R_L}(R_c+R_L)\tfrac{di_2}{dt} + R_c i_2 &= \tfrac{L_c V}{R_L} \\
L_c(R_c+R_L)\tfrac{di_2}{dt} + R_c R_L i_2 &= L_c V \\
\tfrac{di_2}{dt} + \tfrac{R_c R_L}{L_c(R_c+R_L)} i_2 &= \tfrac{L_c V}{L_c(R_c+R_L)} \qquad (3.8) \\
\tfrac{di_2}{dt} &= \tfrac{V}{(R_c+R_L)} - \tfrac{R_c R_L}{L_c(R_c+R_L)} i_2
\end{aligned}
$$

at t = 0,

$$
\begin{aligned}
\frac{di_2}{dt} &= \frac{V}{(R_c+R_L)} \\
\frac{di_2}{dt} &= \frac{V}{R_c}(\because R_L << R_c) \qquad (3.9)
\end{aligned}
$$

put eq. (3.7) in (3.2),

$$
\begin{aligned}
L_c \tfrac{di_1}{dt} &= L_c \tfrac{d}{dt}(\tfrac{V-R_L i_1}{R_c}) - R_L i_1 + V \\
L_c \tfrac{di_1}{dt} &= \tfrac{L_c V}{R_c} - \tfrac{L_c R_L}{R_c}\tfrac{di_1}{dt} - R_L i_1 + V \\
L_c \tfrac{di_1}{dt} + \tfrac{L_c R_L}{R_c}\tfrac{di_1}{dt} + R_L i_1 &= V - (\tfrac{L_c V}{R_c}) \\
L_c(R_c+R_L)\tfrac{di_1}{dt} + R_L R_c i_1 &= (R_c - L_c)V \\
\tfrac{di_1}{dt} + \tfrac{R_L R_c}{L_c(R_c+R_L)} i_1 &= \tfrac{(R_c-L_c)V}{L_c(R_c+R_L)} \qquad (3.10) \\
\tfrac{di_1}{dt} &= \tfrac{(R_c-L_c)V}{L_c(R_c+R_L)} - \tfrac{R_L R_c}{L_c(R_c+R_L)} i_1
\end{aligned}
$$

at t = 0,

$$\begin{aligned} \frac{di_1}{dt} &= \frac{R_c V - L_c V}{L_c(R_c + R_L)} \\ \frac{di_1}{dt} &= \frac{R_c V}{L_c(R_c + R_L)} - \frac{V}{(R_c + R_L)} \\ \frac{di_1}{dt} &= \frac{V}{L_c} - \frac{V}{R_c} (\because R_L << R_c) \end{aligned} \tag{3.11}$$

for expected value of R_c in the order of few ohms and L_c in μH.

$$\frac{di_1}{dt} = \frac{V}{L_c} \tag{3.12}$$

so from eq. (3.9) one can say that, as R_c increases $\frac{di_2}{dt}$ will reduces because R_L is fixed and hence $\frac{di_2}{dt}$ is only depend on R_c.

and from eq. (3.12), it can be said that, as L_c increases $\frac{di_1}{dt}$ decreases.

- Calculation of the i_1

$$\frac{di_2}{dt} + Pi_1 = Q \tag{3.13}$$

from eq. (3.10) and eq. (3.13)

$$P = \frac{R_c R_f}{L_c(R_c + R_f)} \tag{3.14}$$

and

$$Q = \frac{(R_c - L_c)V}{L_c(R_c + R_f)} \tag{3.15}$$

so from first order differential method,

$$i_1 = e^{-Pt}[Q \int e^{Pt} dt + K] \tag{3.16}$$

putting values of P and Q from eq. (3.14) and eq. (3.15) to eq. (3.16)

$$\begin{aligned}
i_1 &= e^{-\frac{R_c R_f t}{L_c(R_c+R_f)}}[\frac{(R_c - L_c)V}{L_c(R_c + R_f)} \int e^{\frac{R_c R_f t}{L_c(R_c+R_f)}} dt + K] \\
i_1 &= e^{-\frac{R_c R_f t}{L_c(R_c+R_f)}}[\frac{(R_c - L_c)V}{L_c(R_c + R_f)} \frac{e^{\frac{R_c R_f t}{L_c(R_c+R_f)}}}{R_c R_f}(L_c(R_c + R_f) + K_1)] \\
i_1 &= \frac{(R_c - L_c)}{R_c R_f} + K_1 e^{-\frac{R_c R_f t}{L_c(R_c+R_f)}} \qquad (3.17)
\end{aligned}$$

now, at t = 0,

$$\begin{aligned}
0 &= \frac{V(R_c - L_c)}{R_c R_f} + K_1 \\
K_1 &= -\frac{V(R_c - L_c)}{R_c R_f} \qquad (3.18)
\end{aligned}$$

put eq. ((3.18)) in to the eq. (3.17),

$$i_1 = \frac{V(R_c - L_c)}{R_c R_f}[1 - e^{-\frac{R_c R_f t}{L_c(R_c+R_f)}}] \tag{3.19}$$

- Calculation of the i_2

$$\frac{di_2}{dt} + Pi_2 = Q \tag{3.20}$$

from eq. (3.8) and eq. (3.20),

(here R_L will be placed by the R_f, because now current will flow through R_f and R_L is short circuited as shown in fig. 3.1)

here

$$P = \frac{R_c R_f}{L_c(R_c + R_f)} \tag{3.21}$$

and

$$Q = \frac{V}{(R_c + R_f)} \tag{3.22}$$

from first order differential method,

$$i_2 = e^{-Pt}[Q \int e^{Pt} dt + K] \tag{3.23}$$

put eq. (3.21) and eq. (3.22) in eq. (3.23),

$$\begin{aligned}
i_2 &= e^{-\frac{R_c R_f}{L_c(R_c+R_f)}t}[\frac{V}{(R_c + R_f)} \int e^{\frac{R_c R_f}{L_c(R_c+R_f)}t} dt + K] \\
i_2 &= e^{-\frac{R_c R_f}{L_c(R_c+R_f)}t}[\frac{V}{(R_c + R_f)} \frac{e^{\frac{R_c R_f}{L_c(R_c+R_f)}t} \times (L_c(R_c + R_f))}{R_c R_f} + K_2] \\
i_2 &= \frac{V L_c}{R_c R_f} + K_2 e^{-\frac{R_c R_f}{L_c(R_c+R_f)}t} \qquad (3.24)
\end{aligned}$$

at t = 0,

$$\begin{aligned}
0 &= \frac{V L_c}{R_c R_f} + K_2 \\
K_2 &= -\frac{V L_c}{R_c R_f} \qquad (3.25)
\end{aligned}$$

put eq. (3.25) in to eq.(3.24),

$$i_2 = \frac{VL_c}{R_c R_f}[1 - e^{-\frac{R_c R_f}{L_c(R_c+R_f)}t}] \tag{3.26}$$

3.1 Simulation Results

Simulation of simplified snubber circuit is performed on Pspice software, to corroborate with the analytical results.

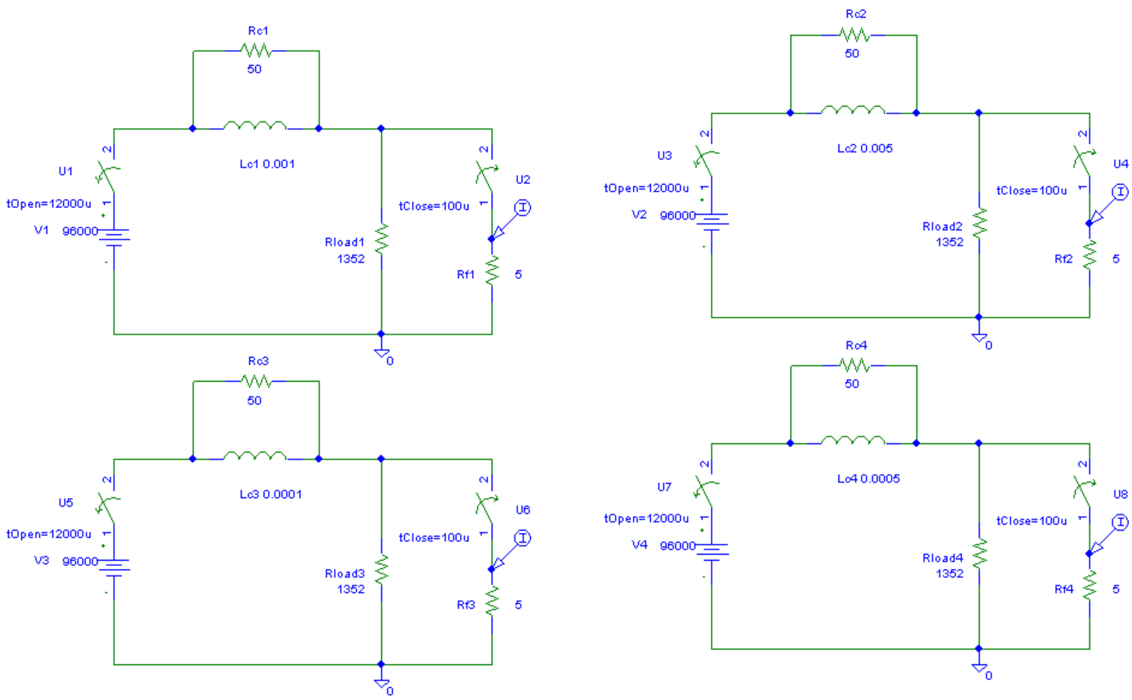

Figure 3.2: Circuit diagram for the observation of the current i_1

Here for the observation of the current i_1, the value of the R_L is fixed and the value of the L_c is varied as depicted in the fig. 3.2. According to the variation in L_c, the value of the current i_1 is observed as shown in fig. 3.3.

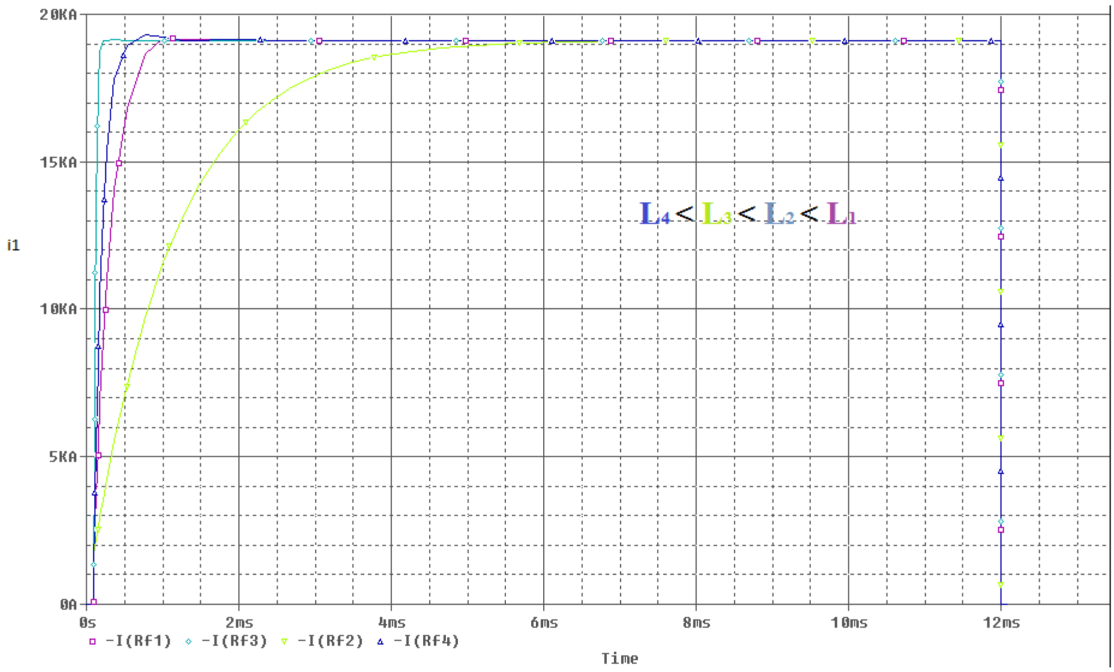

Figure 3.3: Observation results of the current i_1

from the fig. 3.3,it can be said that, for the different values of L_c the current i_1 is in line with the eq. (3.19)

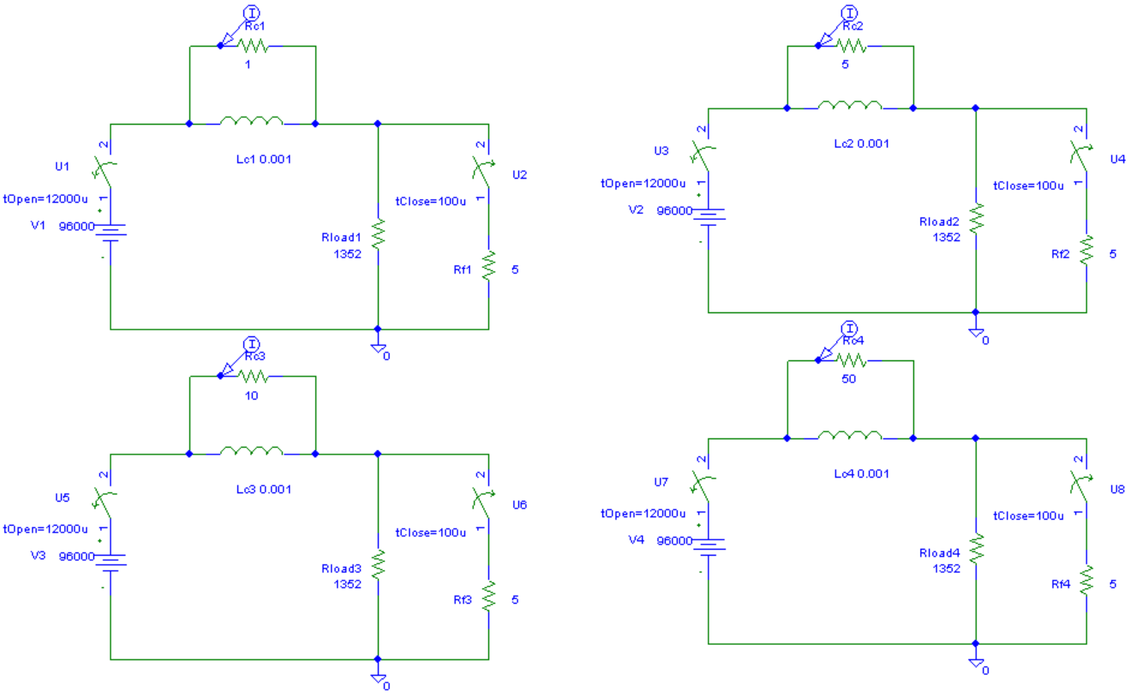

Figure 3.4: Circuit diagram for the observation of the current i_2

Now for the observation of the current i_2, the value of L_c is fixed and the value of R_c is varied as shown in the fig. 3.4. According to the variation in the R_c, the value of the current i_2 is observed as shown in the fig. 3.5.

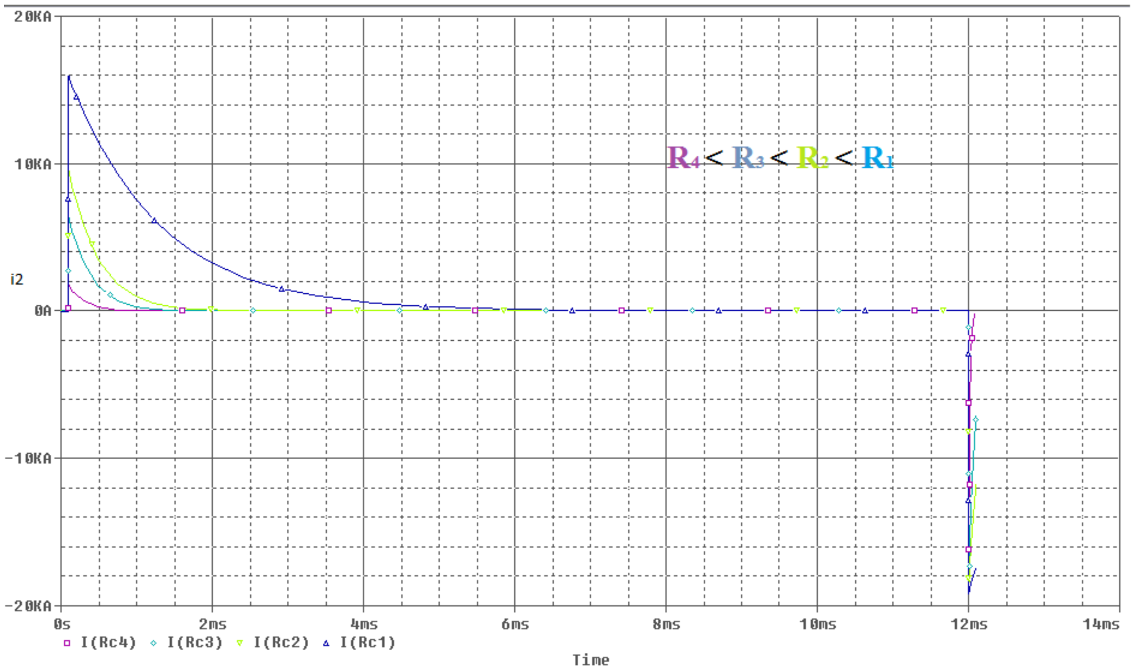

Figure 3.5: Observation results of the current i_2

From fig. 3.5, it can be said that the variation in the R_c will reflected in the behavior of the current i_2, which is in line with the eq. (3.26).

3.2 Energy calculation

If the switch is connected in parallel with the R_L is closed, then short circuit is created through low resistance R_f as shown in fig 3.6.

The energy dissipated by the core can be expressed as,

$$E_c = \int i_2^2 R_c t dt \tag{3.27}$$

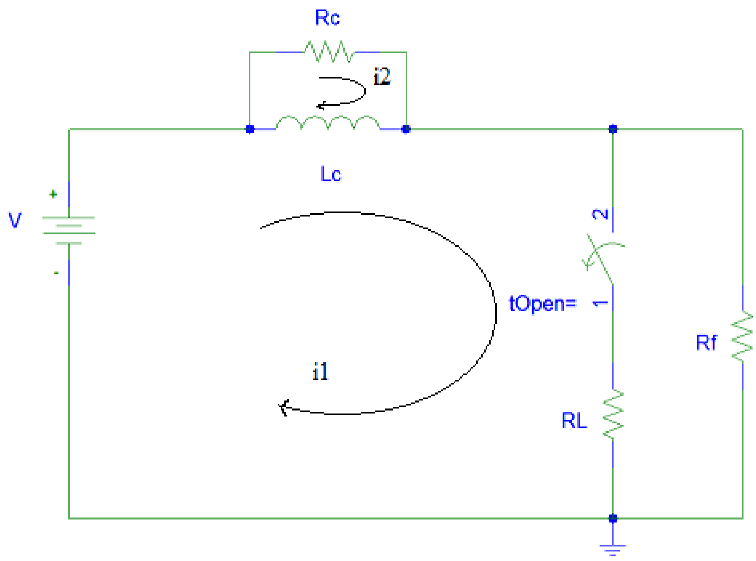

Figure 3.6: Circuit Diagram

The energy dumped in the fault can be expressed as,

$$E_f = \int i_1^2 R_f t dt \tag{3.28}$$

put eq.(3.26) in to eq. (3.27),

$$E_c = \int [\frac{V L_c}{R_c R_f}[1 - e^{-\frac{R_c R_f}{L_c(R_c+R_f)}t}]]^2 R_c t dt \tag{3.29}$$

put eq.(3.19) in to eq. ((3.28)),

$$E_f = \int [\frac{V(R_c - L_c)}{R_c R_f}[1 - e^{-\frac{R_c R_f}{L_c(R_c+R_f)}t}]]^2 R_f t dt \tag{3.30}$$

4

Modeling of snubber

Core snubbers are magnetic disc, encompassing one the current path onward or return, in the present design snubbers are placed on the onward path to prevent voltage lifting of the return conductor.

4.1 Design basis for the core snubbers

Estimation from the simulation indicate the following parameters as shown in table 4.1 to be satisfied by the snubbers:[1]

Parameter	**Value**
Inductance (L_p)	1mH/0.85mH
Resistance (R_p)	2kΩ/1.5kΩ

Table 4.1: Parameters to be satisfied by the snubbers

4.1.1 Physical constraints

The physical constraints are as shown in table 4.2 and the core is as shown in fig. 4.1[1].

ID	670mm
OD	830mm
Width	100mm

Table 4.2: Physical constraint of the snubbers

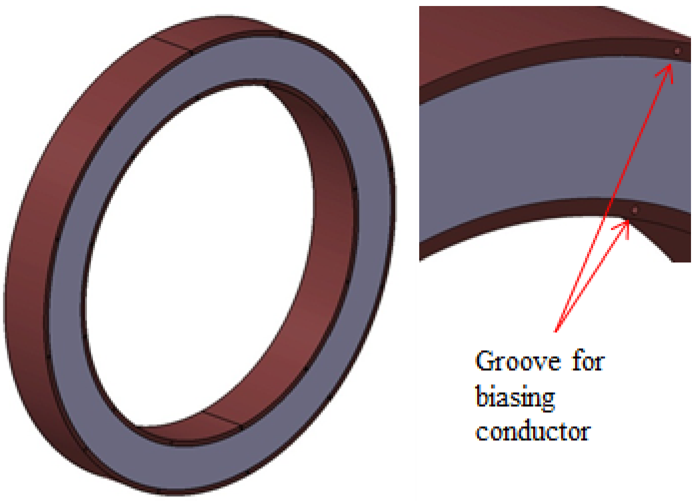

Figure 4.1: Core
[Courtesy: Ongoing experimental work at ITER India]

4.2 Calculation for Inductance

For annular ring, We know that,

$$L = \frac{N\phi}{I} \tag{4.1}$$

but

$$\phi = \int_{r_1}^{r_2} B(r)ds \tag{4.2}$$

for per meter length eq. (4.2) will be,

$$\phi = \int_{r_1}^{r_2} B(r)dr \tag{4.3}$$

we have,

$$B = \frac{\mu_0\mu_r I}{2\pi r}$$

so ϕ will be

$$\begin{aligned}
\phi &= \int_{r_1}^{r_2} \frac{\mu_0\mu_r I}{2\pi r} dr \\
\phi &= \frac{\mu_0\mu_r I}{2\pi} \int_{r_1}^{r_2} \frac{1}{r} dr \\
\phi &= \frac{\mu_0\mu_r I}{2\pi} [\ln r]_{r_1}^{r_2} \\
\phi &= \frac{\mu_0\mu_r I}{2\pi} [\ln r_2 - \ln r_1] \\
\phi &= \frac{\mu_0\mu_r I}{2\pi} [\ln(\frac{r_2}{r_1})]
\end{aligned} \tag{4.4}$$

put eq. (4.4) in to the eq. (4.1)

$$L = \frac{N\mu_0\mu_r}{2\pi} ln(\frac{r_2}{r_1})\ H/m \tag{4.5}$$

4.3 Modeling of snubber

A useful tool for dealing with high frequency magnetic effects is the complex permeability. At high frequencies these quantities will react to each other with some lag time.[2][3] These fields can be written as phasors, such that

$$H = H_0 e^{j\omega t} \qquad B = B_0 e^{j(\omega t - \delta)}$$

Where δ is the phase delay of B from H. Understanding permeability as the ratio of the magnetic field to the auxiliary magnetic field, the ratio of the phasors can be written and simplified as,

$$\mu = \frac{B}{H} = \frac{B_0 e^{j(\omega t - \delta)}}{H_0 e^{j\omega t}} = \frac{B_0}{H_0} e^{-j\delta}$$

So that, the permeability becomes a complex number. By Euler's formula, the complex permeability can be translated from polar to rectangular form,

$$\mu = \frac{B_0}{H_0} \cos\delta - j \frac{B_0}{H_0} \sin\delta = \mu' - j\mu''$$

The ratio of the imaginary to the real part of the complex permeability is called the loss tangent,

$$\tan\delta = \frac{\mu''}{\mu'}$$

Which provides measure of how much power is lost in the material versus how much power is stored. Where, μ' represents the real permeability and indicative of Inductance offered by the core and μ'' represents the imaginary permeability and indicative of loss occurred inside the core material.

4.4 Representation of the magnetic core

- Series Representation

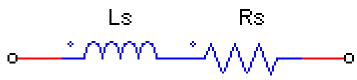

Figure 4.2: Series Representation of the snubber core

$$L_s = L_0\mu'_s \qquad R_s = \omega L_0\mu''_s$$

- Parallel Representation

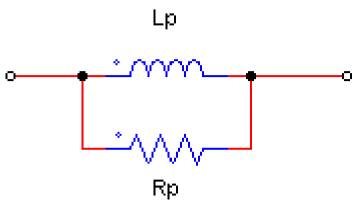

Figure 4.3: Parallel Representation of the snubber core

$$L_p = L_0\mu'_p \qquad R_p = \omega L_0\mu''_p$$

As "L" and "R" are uniformly distributed across whole magnetic core length, it would be more appropriate to represent them as parallel combination in which the voltage across them is same. In fact, losses in the core will be caused due to same voltage appearing across the whole length of magnetic core. The voltage appearing across core will be proportional to its Inductance. Therefore, voltage appearing across "L" and "R" must be same. This condition could be realized with parallel representation of magnetic core for such snubber application.

Transformation of permeability from series model to parallel model [3] or vice versa can be performed as follows

$\mu'_p = \mu'_s(1 + \frac{\mu''^2_s}{\mu'^2_s})$ $\qquad \mu''_p = \mu''_s(1 + \frac{\mu'^2_s}{\mu''^2_s})$

Where,

$L_0 = \frac{\mu_0}{2\pi}\ln(\frac{r_2}{r_1})l$ (from eq. (4.5))

$L_p = L_0\mu'_p$ $\qquad R_p = \omega L_0 \mu''_p$

4.5 Selection of the material

From the fig 4.4, we can say that for our application, as we want either High μ Low Losses or High μ High Losses for that Ferrites, Nanocrystalline, Amorphous, FeSi and NiFe materials can be used. The magnetic and operating properties of the soft magnetic materials (s.m.m.) are as shown in below table 4.3.[4]

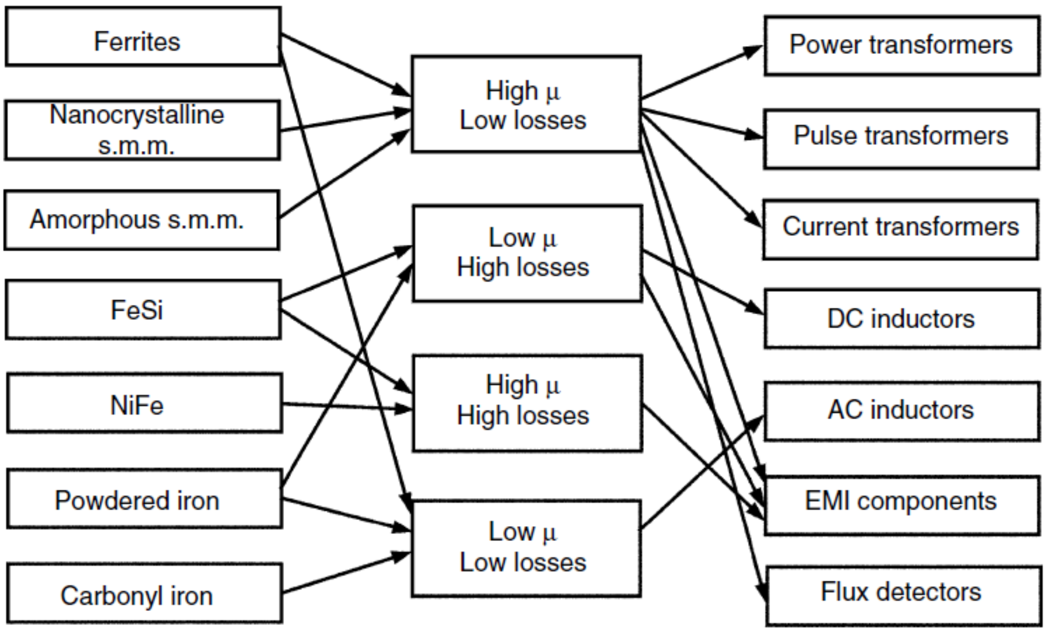

Figure 4.4: Application of various soft magnetic materials

Material	**Ferrites**	**Nano-crystalline**	**Amorphous**	**FeSi Laminated**	**NiFe Laminated**
Contents	MnZn, NiZn bulk	73.5-90% Fe,ribbon thickness 20 μm	73.5% Fe,ribbon thickness 5-25 μm	3-6% Si	Permalloy: 80% Ni
Permeability, μ	100-20000	**15000-20000**	10000-15000	1000-10000	10000
B_{peak}, T	0.3-0.45	**1.2-1.5**	0.7-1.8	1.9	1
ρ, $\mu\Omega$m	$10^2 to 10^9$MnZn $10^7 to 10^9$NiZn	0.4-1.2	1.2-2	0.4-0.7	0.15
P_{loss}, W/kg	12at 0.2T/20kHz	5at 0.2T/20kHz	18at 0.2T/20kHz	0.3-3at 1.5T/50Hz	24at 0.2T/5kHz
Curie temp.T_c,^0C	125-450	600	350-450	720	500

Table 4.3: Magnetic and Operating Property of s.m.m.

4.6 Estimation of L_P, R_P for a magnetic core

From $FINEMET^{®}$ datasheet,[5]

at f = 500kHz,

$\mu'_S = 3000$

$\mu''_S = 6000$

Now,

$$\mu'_P = \mu'_S(1 + \frac{\mu''^2_S}{\mu'^2_S}) = 3000(1 + \frac{6000^2}{3000^2}) = 15000$$

$$\mu''_P = \mu''_S(1 + \frac{\mu'^2_S}{\mu''^2_S}) = 6000(1 + \frac{3000^2}{6000^2}) = 7500$$

for a magnetic core of following dimensions,

Inner Diameter of the snubber core = 670 mm $\Rightarrow$ $r_1 = 335\ mm$

Outer Diameter of the snubber core = 830 mm $\Rightarrow$ $r_2 = 415\ mm$

Height of the snubber core = 100 mm $\Rightarrow$ $l = 100\ mm$

from eq. (4.5), the inductance can be calculated as,

$$
\begin{aligned}
L_0 &= \tfrac{\mu_0}{2\pi}\ln(\tfrac{r_2}{r_1})l\ H \\
&= \tfrac{4\pi\times10^{-7}}{2\pi}\ln(\tfrac{415}{335})0.1 \\
&= 4.3\times10^{-9}H
\end{aligned}
$$

For Parallel representation,

$$
\begin{aligned}
L_P &= L_0\mu'_P & R_P &= \omega L_0\mu''_P \\
&= 4.3\times10^{-9}\times15000 & &= 2\times\pi\times500\times10^3\times4.3\times10^{-}9\times7500 \\
&= 65\mu H & &= 101\Omega
\end{aligned}
$$

Parameters offered from Single disc	13♯ **discs suffice**
$L_p = 65\ \mu H$	$L_p = 850\ \mu H$
$R_p = 101\ \Omega$	$R_p = 1.5\ k\Omega$

Table 4.4: Parameters offered by the FINEMET at 500 kHz

5

Experimental configuration and results

From the comparison of the materials (section 4.6) it can be concluded that the FINEMET material offers required performance parameters for particular application but is not easily available in the market for the required dimensions. CRGO material on the other hand is common and selected for the case study of snubber cores. Aim of the experiment is to characterize the actual size CRGO snubbers on the same line as the high frequency performance material like FINEMET, complex permeability data at high frequency is normally not available from the CRGO supplier in India. A relative data shall be helpful while finalising the material selection. Besides that on experimental setup will be established for future characterizations.

5.1 Deployment of snubber

As already discussed in section 4.1.1 the physical constraints of the core snubbers has to match with the Transmission line provisions, this suggests the snubber to be annular ring (disc) or set of annular rings as shown in fig 5.1[6].

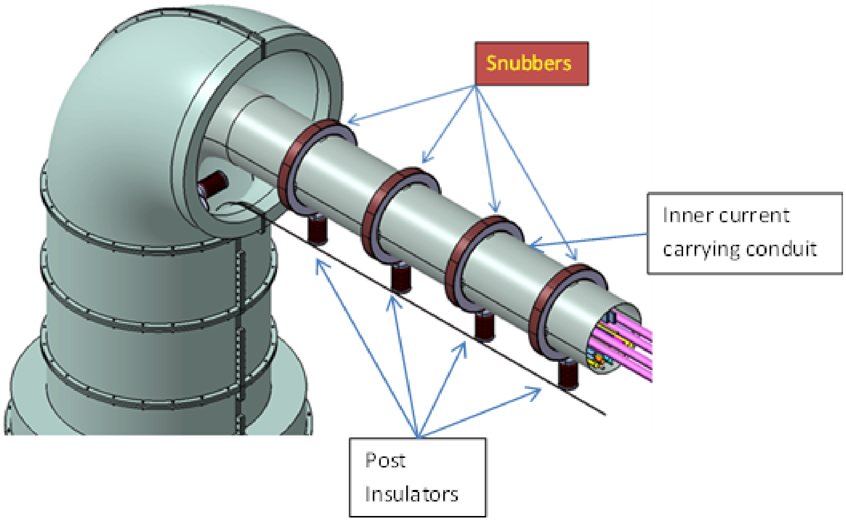

Figure 5.1: Snubber deployment on Transmission Line
[Courtesy: ITER-India Power Supply Team]

5.2 Snubber Core

Figure 5.2: Snubber Core
[Courtesy: Ongoing experimental work at ITER India]

The snubber core used is as shown in fig.5.2.

The details of the snubber core is given below:

Inner Diameter: 650mm (670mm keeping provision for biasing winding)

Outer Diameter: 850mm (830mm keeping provision for biasing winding)

Width: 100mm Height: 50mm

Material: CRGO (M-6 Grade-0.35mm thickness)

Flux Density(B): 1.3T at 50Hz

A number of snubber cores are used throughout the TL at regular interval to introduce inductance during grid breakdown condition. The inductance introduced during breakdown condition is limiting the energy and controlling the fault current decay time. Number of snubber cores are decide value of total inductance introduced in the TL. Hence number of snubber cores are decide the energy limit and fault current decay time.

5.3 Cylinder

Figure 5.3: Cylinder representing inner current carrying conduit
[Courtesy: Ongoing experimental work at ITER India]

The Cylinder used is as shown in fig.5.3.
The details of the cylinder is given below:
Diameter: 649mm
Height: 1500mm
Material: Stainless Steel (SS304-1mm thickness)

Cylinder is used as a part of the transmission line for shielding individual objects passing through the TL. Therefore, to match with the TL assembly (as shown in fig. 5.4) cylinder is used. Cylinder is placed in the core as shown in fig. 5.5Cylinder minimizes the air gap between snubber core and the cylinder, that results in reduction of the leakage flux and hence improve the magnetic coupling.

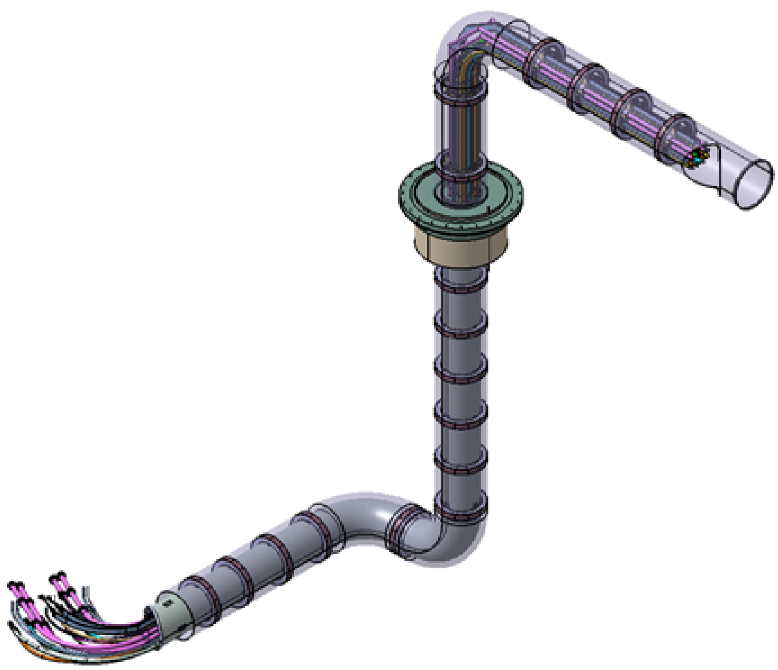

Figure 5.4: Cylinder as a part of TL
[Courtesy: ITER-India Power Supply Team]

Figure 5.5: Cylinder in the core
[Courtesy: Ongoing experimental work at ITER India]

5.4 Single Snubber core assembled on the TL

The single snubber core is assembled on the TL as shown in fig.5.6. Single snubber core is supported by epoxy resin insulator of 33kV, this whole assembly placed on the main supporting structure of the TL made up of stainless steel.

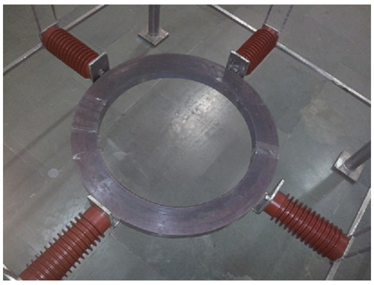

Figure 5.6: Single Snubber core assembled on the TL
[Courtesy: Ongoing experimental work at ITER India]

Two snubber cores are separated by 1m. This assembly is used to compute incremental data of the inductance due to adding one more snubber as shown in fig.5.7

Figure 5.7: Prototype transmission model with two snubber core
[Courtesy: Ongoing experimental work at ITER India]

5.5 Observed results

Measurement of inductance due to single snubber core is done by arrangement as shown in fig.5.8.

Figure 5.8: Inductance measurement of the Snubber
[Courtesy: Ongoing experimental work at ITER India]

The Values for the inductances (Series and parallel), resistances (Series and parallel), impedance and the theta (the angle between real and imaginary axis of the impedance) are observed as shown in table 5.1 and table 5.2 for expected range of fault current frequency (1MHz and 500kHz) respectively.

Description	R_s (Ω)	R_p (Ω)	L_s (μH)	L_p (μH)	**Z (Ω)**	**Theta (^{0})**
Only Cylinder	0.525	105.125	1.17	1.17	7.15	90.505
Cylinder in the core	0.623	130.145	1.43	1.43	9	86.029

Table 5.1: Parameters at 1MHz frequency

Description	R_s (Ω)	R_p (Ω)	L_s (μH)	L_p (μH)	**Z (Ω)**	**Theta (^{0})**
Only Cylinder	0.0158	825.94	1.15	1.15	3.62	89.748
Cylinder in the core	0.502	43.555	1.48	1.48	4.68	83.852

Table 5.2: Parameters at 500kHz frequency

As a result of the testing the following graphs are observed. Which is shown from fig, 5.9 to 5.12 for different configurations

- Cylinder

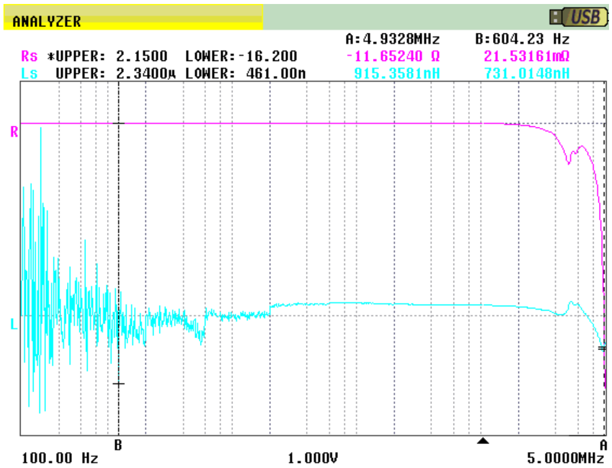

Figure 5.9: R_s Vs L_s for cylinder without core

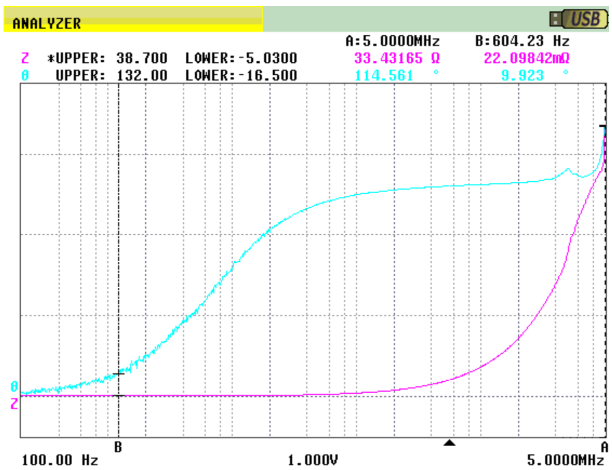

Figure 5.10: Z Vs θ for cylinder without core

- Cylinder in core

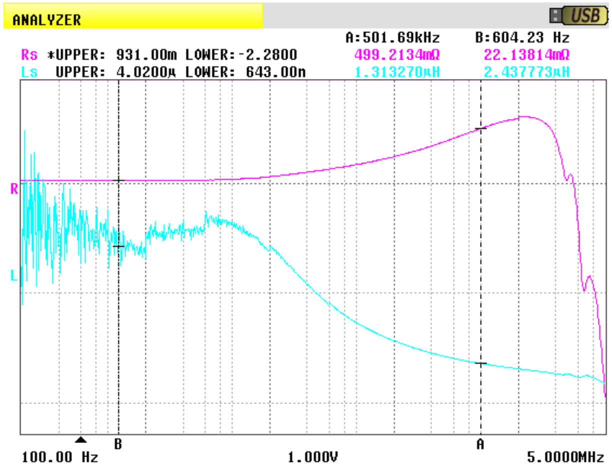

Figure 5.11: R_s Vs L_s for cylinder in core

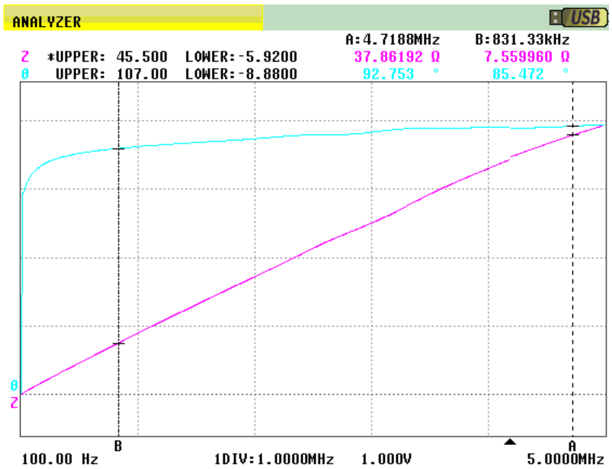

Figure 5.12: Z Vs θ for cylinder in core

5.6 calculation for μ_p' and μ_p''

- At f = 500kHz,

$$
\begin{aligned}
L_0 &= \frac{\mu_0}{2\pi}\ln(\frac{r_2}{r_1})l \qquad \text{(from eq. (4.5))} \\
&= 2\times 10^{-7}\ln(\frac{415}{335})0.05 \\
&= 2.141\ nH
\end{aligned}
$$

Now

$$
\begin{aligned}
L_S &= L_0\mu_S' \\
\mu_S' &= \frac{L_S}{L_0} \\
&= \frac{1.48\times10^{-6}}{2.141\times10^{-9}} \\
&= 691.2657
\end{aligned}
\qquad
\begin{aligned}
R_S &= \omega L_0\mu_S'' \\
\mu_S'' &= \frac{R_S}{\omega L_0} \\
&= \frac{0.502}{2\pi\times500\times10^3\times2.141\times10^{-9}} \\
&= 74.6341
\end{aligned}
$$

Therefore,

$$
\begin{aligned}
\mu_P' &= \mu_S'(1+\frac{\mu_S''^2}{\mu_S'^2}) \\
&= 691.2657(1+\frac{74.6341^2}{691.2657^2}) \\
&= 699.3238
\end{aligned}
\qquad
\begin{aligned}
\mu_P'' &= \mu_S''(1+\frac{\mu_S'^2}{\mu_S''^2}) \\
&= 74.6341(1+\frac{691.2657^2}{74.6341^2}) \\
&= 6477.1832
\end{aligned}
$$

- At f = 1MHz,

  $L_0 = 2.141\ nH$

  Now

$$L_S = L_0\mu'_S \qquad R_S = \omega L_0\mu''_S$$

$$\mu'_S = \frac{L_S}{L_0} = \frac{1.43\times10^{-6}}{2.141\times10^{-9}} = 667.9122 \qquad \mu''_S = \frac{R_S}{\omega L_0} = \frac{0.623}{2\pi\times1\times10^{6}\times2.141\times10^{-9}} = 46.3118$$

Therefore,

$$\mu'_P = \mu'_S(1+\frac{\mu''^2_S}{\mu'^2_S}) = 667.9122(1+\frac{46.3118^2}{667.9122^2}) = 671.1234$$

$$\mu''_P = \mu''_S(1+\frac{\mu'^2_S}{\mu''^2_S}) = 46.3118(1+\frac{667.9122^2}{46.3118^2}) = 9678.9942$$

The calculation of μ'_P and μ''_P for CRGO at 1MHz and 500kHz is summarized as shown in table 5.3.

Description	μ'_P	μ''_P
at 500kHz	699.3238	6477.1832
at 1MHz	671.1234	9678.9942

Table 5.3: Values of μ'_P and μ''_P for CRGO at 1MHz and 500kHz

Parameters offered from Single disc	570♯ **discs suffice**
$L_p = 1.46\ \mu H$	$L_p = 850\ \mu H$
$R_p = 43.52\ \Omega$	$R_p = 1.5\ k\Omega$

Table 5.4: Parameters offered by the CRGO at 500 kHz

6

Saturation Current Calculation

In the normal operating condition, a DC current of 75A will flow through the snubber. Saturation of the core snubber must be avoided to obtain their expected performance during the peak fault current. It is therefore important to assess the effect of 75A DC on the saturation characteristics of the core and to device corresponding reverse biasing. Both CRGO as well as FINEMET is considered for their saturation assessment.

The saturation magnetic flux density is $B_{sat} = 1.5$T (for CRGO) and $B_{sat} = 1.2$ T (for FINEMET) , according to the core datasheet.
The saturation flux for a single core is,

$$\phi_{sat} = B_{sat} * A_e \tag{6.1}$$

To facilitate design and application, a magnetic core having the nonuniform flux distribution is approximated by an idealized core with uniform flux distribution. This can be characterized by effective area A_e.[7]

$$A_e = \frac{C_1}{C_2}[8][9] \tag{6.2}$$

where,

$$C_1 = \frac{2\pi}{h\ln\left(\frac{r_2}{r_1}\right)} \qquad C_2 = \frac{2\pi\left[\left(\frac{1}{r_1}\right)-\left(\frac{1}{r_2}\right)\right]}{h^2\ln^3\left(\frac{r_2}{r_1}\right)} [8][9] \tag{6.3}$$

by putting eq. (6.3) in eq. (6.2) we get,

$$A_e = \frac{h\ln^2\left(\frac{r_2}{r_1}\right)}{\left(\frac{1}{r_1}\right)-\left(\frac{1}{r_2}\right)} \tag{6.4}$$

We have

$r_2 = 415\ mm$

$r_1 = 335\ mm$

$h = 50\ mm$

so, from eq. (6.4)

$$\begin{aligned} A_e &= \frac{h\ln^2\left(\frac{r_2}{r_1}\right)}{\left(\frac{1}{r_1}\right)-\left(\frac{1}{r_2}\right)} \\ &= \frac{0.05\ln^2\left(\frac{0.415}{0.335}\right)}{\left(\frac{1}{0.335}\right)-\left(\frac{1}{0.415}\right)} \\ &= 0.003985\ m^2 \end{aligned}$$

Substituting the value of A_e *and* B_{sat} in eq. (6.1),

For FINEMET,

$$\begin{aligned} \phi_{sat} &= B_{sat} * A_e \\ &= 1.2 * 0.003985 \\ &= 0.004782\ Wb \end{aligned} \tag{6.5}$$

For CRGO,

$$\begin{aligned} \phi_{sat} &= B_{sat} * A_e \\ &= 1.5 * 0.003985 \\ &= 0.005977\ Wb \end{aligned} \tag{6.6}$$

The saturation current i.e. the maximum current corresponding to the value of saturation flux is computed from the DC core inductivity,[10]

$$L_{DC} = \frac{\mu_0 \mu_r}{2\pi} \ln\left(\frac{r_2}{r_1}\right) h$$

For FINEMET, $\mu_r = 70000$ (taken from the datasheet)
so,

$$\begin{aligned} L_{DC} &= \tfrac{\mu_0 \mu_r}{2\pi} \ln\left(\tfrac{r_2}{r_1}\right) h \\ &= \tfrac{4\pi \times 10^{-7} \times 70000}{2\pi} \ln\left(\tfrac{0.415}{0.335}\right) 0.05 \\ &= 0.00015\ H \end{aligned} \tag{6.7}$$

For CRGO, $\mu_r = 9032.234$ (taken from the observations)
so,

$$\begin{aligned} L_{DC} &= \tfrac{\mu_0 \mu_r}{2\pi} \ln\left(\tfrac{r_2}{r_1}\right) h \\ &= \tfrac{4\pi \times 10^{-7} \times 9032.234}{2\pi} \ln\left(\tfrac{0.415}{0.335}\right) 0.05 \\ &= 1.93 \times 10^{-5}\ H \end{aligned} \tag{6.8}$$

So from eq. (6.5) and (6.7) the saturation current for FINEMET is,

$$I_{sat} = \frac{\phi_{sat}}{L_{DC}} = \frac{0.004782}{0.00015} = 31.89\ A < 75\ A \tag{6.9}$$

and from eq. (6.6) and (6.8) the saturation current for CRGO is,

$$I_{sat} = \frac{\phi_{sat}}{L_{DC}} = \frac{0.005977}{1.93 \times 10^{-5}} = 309.0174\ A \gg 75\ A \tag{6.10}$$

Definitely CRGO offers higher saturation limits than FINEMET for the conditions. But CRGO indicates the dense deployment of the snubbers on the transmission line having the length of approximately 150m.

Therefore FINEMET material is considered for the snubber core.

7

Representation of the Snubber core as Magnetic element

As magnetic materials display strong dependency on excitation frequency and presence of DC component, magnetic element of PSIM tool is analysed for mapping the behaviour and discussed in this chapter.

7.1 Introduction to the saturable core

The magnetic elements in PSIM (windings, leakage paths, air gaps, and magnetic cores) provides a powerful way of modeling magnetic devices. The Typical saturable core element presents the following parameters:[11]

Inductance Factor AL	Inductance factor AL of the core, in H, defined as the inductance per turn squared.
Resistance for Losses	Resistance R, in Ohm, that represents the core losses
Coefficient ϕ_{sat}	Coefficient ϕ_{sat} for the core B-H curve
Coefficient K_1	Coefficient K_1 for the core B-H curve
Coefficient K_{exp1}	Coefficient K_{exp1} for the core B-H curve
Coefficient K_2	Coefficient K_2 for the core B-H curve
Coefficient K_{exp2}	Coefficient K_{exp2} for the core B-H curve
Current Flag	Flag of the electric current that flows through the resistor R for the core losses. If the rms value of the current is $Irms$, the core losses can be calculated as: $P_{core_loss} = I_{rms}^2 R$.

Table 7.1: Saturable core element parameters

The simulated B-H curve of the saturable core depends on the combined effect of all the parameters 7.1. The diagram 7.1 shows how the parameters are related to the B-H curve.

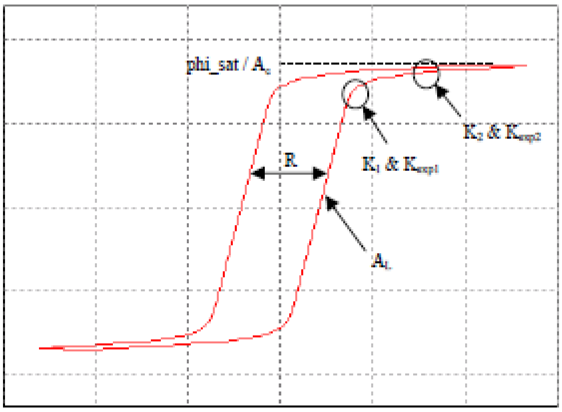

Figure 7.1: The B-H curve of the saturable core

The **inductance factor *AL*** mainly affects the slope of the linear region. A larger value of A_L will result in a steeper slope. A_L can be found out by:

$$AL = \frac{\mu_0 \mu_r A_e}{L_m}$$

The **resistance R** determines the width of the hysteresis loop. The larger the resistance, the wider the hysteresis loop.

The **coefficient** $\boldsymbol{\phi_{sat}}$ is roughly equal to the core flux at the deep saturation, It can be calculated as the flux density B at the deep saturation multiplied by the core cross section area A_e.

The **coefficient** $\boldsymbol{K_1}$ determine when the B-H curve starts to saturate means the first knee point. It can be found out by taking the ratio of the flux density at this point to the flux density at deep saturation.

The **coefficient** $\boldsymbol{K_{exp1}}$ determines how sharp the transition of the curve is around this point. The larger the value of K_{exp1}, the sharper the transition.

The **coefficient** $\boldsymbol{K_2}$ and $\boldsymbol{K_{exp2}}$ associated with the second knee point in the saturation region, and are used mainly to better fit the curve in the saturation region. It can be found out by taking the ratio of the flux density at this point to the flux density at deep saturation.

7.2 Representation of the Snubber core as Saturable core

B-H curve for the FT-3M type core of FINEMET[5] is considered as the reference for developing the saturable core model.Typical datasheet values for FT-3M type core provides complex permeability for excitation level of H=0.05AT/m at 100kHz. Subsequently R_s and L_s for the core can be obtained analytically.[3]

As an initial attempt, the saturable core element is attributed to display the same impedance parameters namely R_s and L_s as the FT-3M. For DC condition the core is excited at lower frequency as 1 Hz. The resultant B-H curve is as shown in fig. 7.4 indicates achievable maximum flux density $\sim$ 1.2T.

Once validated on the lower excitation levels (H=0.05AT/m as shown in fig. 7.3), the saturable core model was excited to the desired level of 500AT/m and its offered impedance parameters were observed.

Simulation (7.2) is done for the parameters given in the datasheet, for that the resultant B-H curve for the FINEMET is as shown in fig. 7.3.

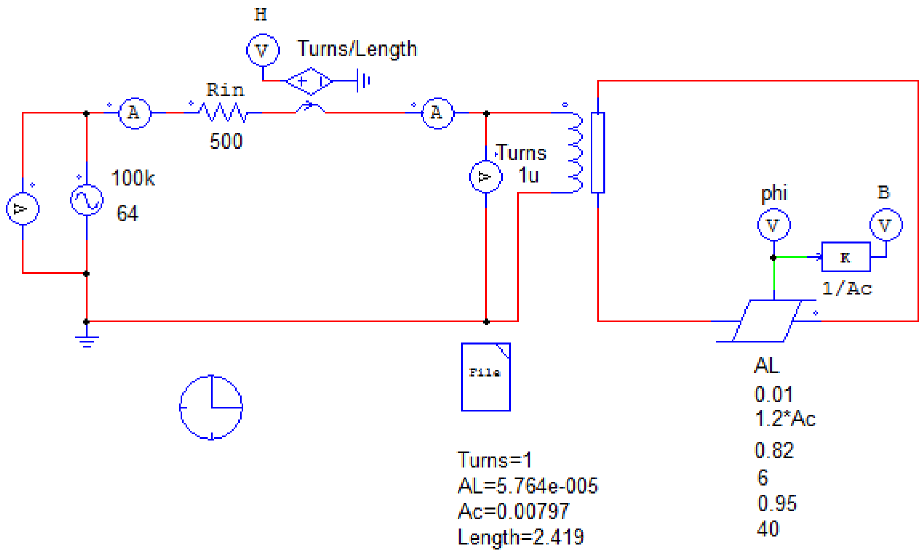

Figure 7.2: Simulation circuit diagram

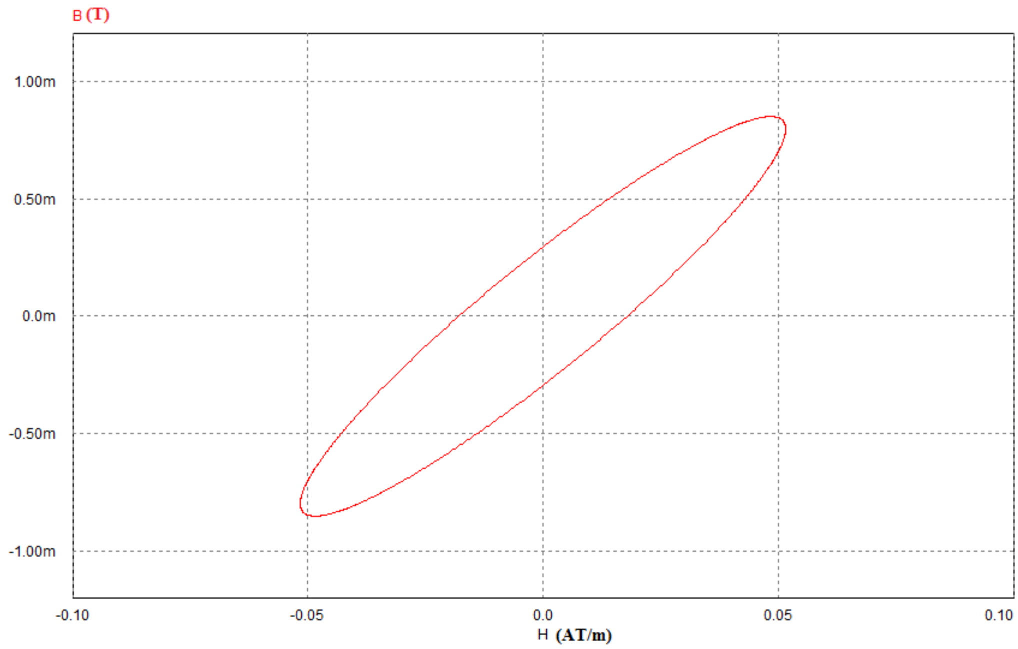

Figure 7.3: B-H curve at lower excitation (H=0.05AT/m)

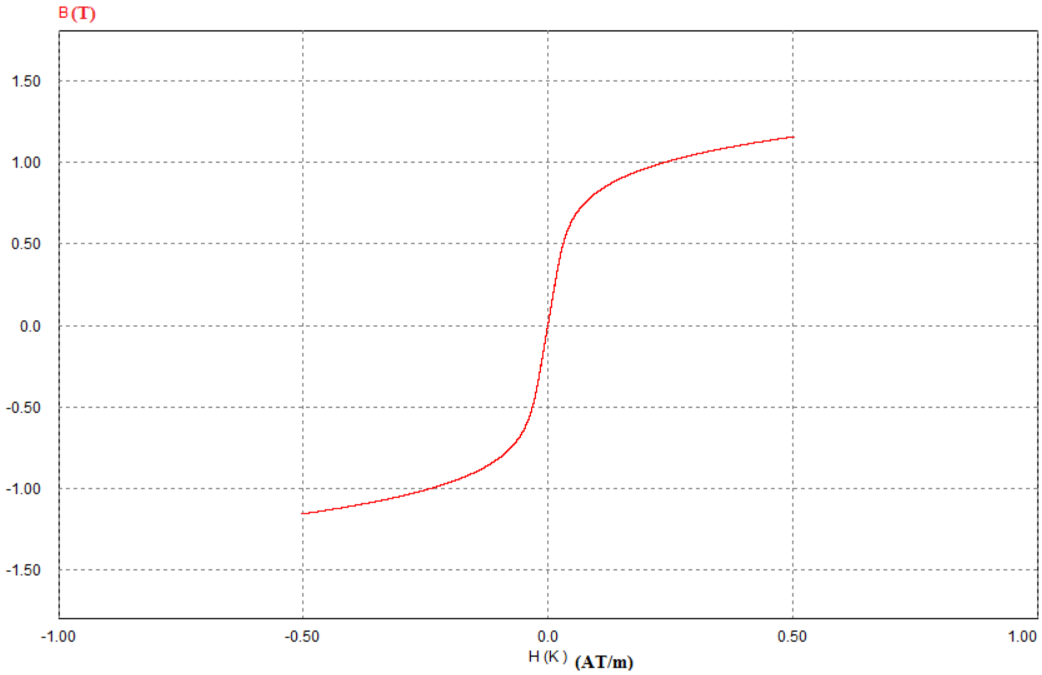

Figure 7.4: B-H curve at DC condition

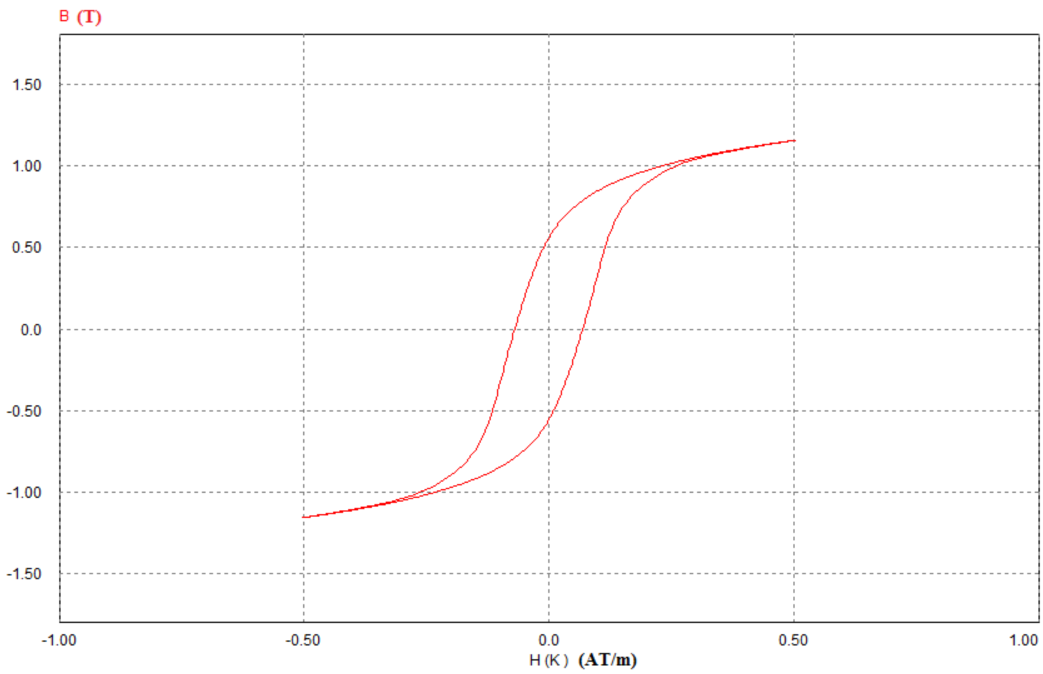

Figure 7.5: B-H curve at higher excitation (H=500AT/m)

7.3 Comparison of Impedance Parameters @ lower excitation

For FT-3M type FINEMET material, offered impedance from the model is compared with calculated parameters.[3].

From $FINEMET^{®}$ datasheet,[5]
at f = 100kHz,
$\mu'_S = 14000$
$\mu''_S = 18000$
for a magnetic core of following dimensions,
Inner Diameter of the snubber core = 670 mm $\Rightarrow\ r_1 \ = \ 335\ mm$
Outer Diameter of the snubber core = 830 mm $\Rightarrow\ r_2 \ = \ 415\ mm$
Height of the snubber core = 100 mm $\Rightarrow\ l \ = \ 100\ mm$

$$L_m \ = \ 2\pi r_{avg} \ = \ 2\pi(0.335 + 0.05) \ = \ 2.419\ m \tag{7.1}$$

$$A_e \ = \ \frac{h\ln^2\left(\frac{r_2}{r_1}\right)}{\left(\frac{1}{r_1}\right) - \left(\frac{1}{r_2}\right)} \ = \ \frac{0.1\ln^2\left(\frac{0.415}{0.335}\right)}{\left(\frac{1}{0.335}\right) - \left(\frac{1}{0.415}\right)} \ = \ 0.00797\ m^2 \tag{7.2}$$

$$AL \ = \ \frac{\mu_0\mu_r A_e}{L_m} \ = \ \frac{4\pi\times10^{-7}\times14000\times0.00797}{2.419} \ = \ 5.7964\times10^{-5}\ m^2 \tag{7.3}$$

7.3.1 Calculated Impedance Parameters

From eq. (4.5), the inductance can be calculated as,

$$L_0 \ = \ \frac{\mu_0}{2\pi}\ln(\frac{r_2}{r_1})l\ H \ = \ \frac{4\pi\times10^{-7}}{2\pi}\ln(\frac{0.415}{0.335})0.1 \ = \ 4.3\times10^{-9}\ H$$

$$L_S \ = \ L_0\mu'_S \ = \ 4.3\times10^{-9}\times14000 \ = \ 60.2\ \mu H \tag{7.4}$$

$$R_S \ = \ \omega L_0\mu''_S \ = \ 2\pi\times100\times10^3\times4.3\times10^{-9}\times18000 \ = \ 48.63\ \Omega \tag{7.5}$$

7.3.2 Impedance achieved from the Model

For f = 100 kHz,

Inductance Factor AL	$5.7964 \times 10^{-5}\ H^2/m$
Resistance for Losses	$1 \times 10^{-12}\ \Omega$
Coefficient ϕ_{sat}	1.2*0.00797 Wb
Coefficient K_1	0.66
Coefficient K_{exp1}	6
Coefficient K_2	1.3
Coefficient K_{exp2}	40
Current Flag	1

Table 7.2: Saturable core element parameters of the Model

From the simulation (7.2), the voltage across the Saturable core element (V_m) and current through it (I_m) is observed,

$V_m \ = \ 4.62354\ V$

$I_m \ = \ 0.127664\ A$

so $Z \ = \ \frac{V_m}{I_m} \ = \ 36.2164745\Omega$

now for the phase angle,

$\phi \ = \ 360 * \Delta t * f$ (where measured $\Delta t \ = \ 25 \times 10^{-7}\ seconds$)

$= \ 90$

$\cos\phi \ = \ 0$

$$R_S \ = \ Z * \cos\phi \ = \ 0\ \Omega \tag{7.6}$$

$\sin\phi \ = \ 1$

$$X_L \ = \ Z * \sin\phi \ = \ 36.2164745\ \mu H$$

$$L_S \ = \ \frac{X_L}{2\pi f} \ = \ 5.76403 \times 10^{-5}\ \mu H \tag{7.7}$$

From eq. (7.5) & (7.6) and (7.4) & (7.7), it is observed that the parameters offered by the model differ from the expected value of R_S although L_S matches closely. Attributes to the model need to be fine tuned for achieving the desired performance.

R_C is scanned from $n\Omega$ to few ohms to see the achievable R_S. The results are as shown in the table 7.3.

R_c	V_m	I_m	Z	R_S	L_S
1×10^{-9}	4.62354	0.127664	36.2164745	0	5.76403×10^{-5}
1×10^{-8}	4.62354	0.127664	36.2164745	0	5.76403×10^{-5}
1×10^{-7}	4.62354	0.127664	36.2164745	0	5.76403×10^{-5}
1×10^{-6}	4.62353	0.127664	36.21639616	0	5.76402×10^{-5}
1×10^{-5}	4.62342	0.127661	36.21638558	0	5.76402×10^{-5}
2×10^{-5}	4.62331	0.127658	36.52480645	0	5.76402×10^{-5}
3×10^{-5}	4.62319	0.127654	36.53540382	0	5.76405×10^{-5}
4×10^{-5}	4.62307	0.127651	36.21648087	0	5.76403×10^{-5}
5×10^{-5}	4.62295	0.127648	36.21639195	0	5.76402×10^{-5}
6×10^{-5}	4.62282	0.127644	36.21650841	0	5.76404×10^{-5}
7×10^{-5}	4.6227	0.127641	36.21641949	0	5.76402×10^{-5}
8×10^{-5}	4.62258	0.127638	36.21633056	0	5.76401×10^{-5}
8.1×10^{-5}	4.62256	0.127637	36.21645761	0	5.76403×10^{-5}
8.2×10^{-5}	4.62255	0.127637	36.21637926	0	5.76402×10^{-5}
8.3×10^{-5}	4.62254	0.127637	36.21630092	0	5.764×10^{-5}
8.35×10^{-5}	4.62253	0.127636	36.21650631	0	5.76404×10^{-5}
8.4×10^{-5}	4.62253	0.127636	36.21650631	0.227553524	5.7629×10^{-5}
8.5×10^{-5}	4.62251	0.127636	36.21634962	0.227547325	5.7639×10^{-5}
9×10^{-5}	4.62245	0.127634	36.21644703	0.227547937	5.76391×10^{-5}
9.5×10^{-5}	4.62239	0.127633	36.21626068	0.227546766	5.76388×10^{-5}
9.8×10^{-5}	4.62235	0.127632	36.21623104	0.22754658	5.76388×10^{-5}
0.0001	4.62232	0.127631	36.21627974	0.227546886	5.76389×10^{-5}
0.001	4.60854	0.127333	36.19281726	1.364107282	5.75617×10^{-5}
0.01	4.26143	0.124854	34.13130536	11.76301308	5.09936×10^{-5}
0.02	3.62547	0.123611	29.32967131	**18.29417717**	$\mathbf{3.64859 \times 10^{-5}}$
0.03	3.02833	0.123478	24.52525956	17.98314657	2.65406×10^{-5}
0.1	1.21128	0.125663	9.639114139	9.289435995	4.09458×10^{-6}
0.5	0.254594	0.127492	1.99640985	1.993745879	1.79634×10^{-7}

Table 7.3: Simulated Results for different value of core loss resistances R_C

From the table 7.3 and plot 7.6, it can be seen that the highest achievable R_S is 18 Ω (at $R_C = 0.02$ Ω)as against the required value of 40 Ω.

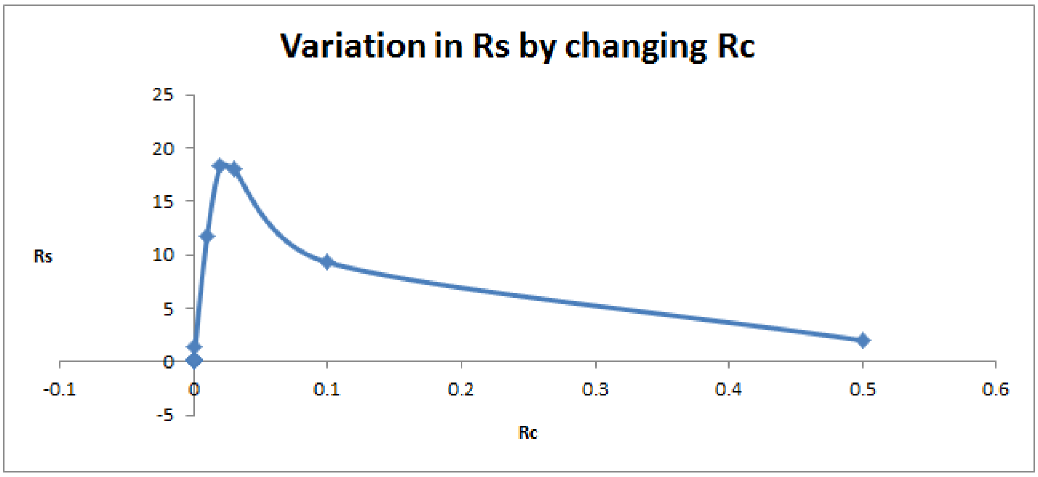

Figure 7.6: Variation of R_S by changing R_C

At this value of R_C, AL is varied in a range of ± 5% from the calculated value to see the behavior of R_S as shown in table 7.4 and plot 7.7.

AL	$\boldsymbol{V}_m$	$\boldsymbol{I}_m$	**Z**	$\boldsymbol{R}_S$	$\boldsymbol{L}_S$
5.4×10^{-5}	3.48018	0.123962	28.07457124	15.92640948	3.6797×10^{-5}
5.5×10^{-5}	3.52114	0.123864	28.42746884	16.12660458	3.72597×10^{-5}
5.764×10^{-5}	3.62547	0.123611	29.32967131	**18.29417717**	$\mathbf{3.64859 \times 10^{-5}}$
5.8×10^{-5}	3.63925	0.123577	29.44925027	17.30983346	3.79186×10^{-5}
5.9×10^{-5}	3.67707	0.123483	29.77794514	17.65405786	3.8166×10^{-5}
5.95×10^{-5}	3.48018	0.123962	28.07457124	15.78024981	3.69557×10^{-5}
6×10^{-5}	3.71412	2.24319	1.655731347	0.998289341	2.10233×10^{-6}

Table 7.4: Simulated Results for different value of AL

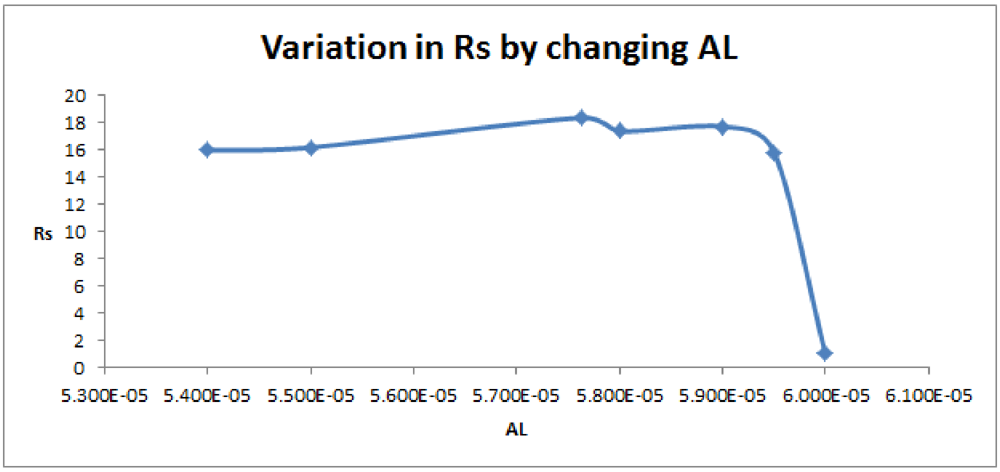

Figure 7.7: Variation of R_S by changing AL

From the table 7.3 & 7.4 and plot 7.6 & 7.7, it is observed that the highest achievable value of R_S is only 18 Ω, such behavior from the model suggest limitation of the saturable core element.

8

Conclusion and Future Work

8.1 Conclusion

The present project work attempts to achieve the targets where snubbers for limiting and mitigating the fault energy during the fault conditions are realised as annular magnetic discs. Representation of the snubbers is realised with high frequency circuit parameters, where individual magnetic disc corresponds to equivalent impedance.

With the given physical constraints coming from the layout of the transmission line, possible deployment scheme for the snubbers is presented.

Experimental work has been carried out at the ITER-India lab to assess the behaviour of actual size snubbers. A case study of snubber with CRGO material is discussed. The material is characterised at the fault frequency range 500kHz-1MHz. As expected lower μ'_p for the CRGO indicates the dense deployment of the snubbers on the TL. High frequency performance nano-crytalline material on the other hand can offer compact solution.

Under the normal operating conditions of DC current, assessment of saturation characteristics allows higher limits for the CRGO whereas nano-crysatlline shall need DC biasing.

The developed saturable core model with PSIM has been assessed for lower excitation levels, however lacks corroboration with estimated performance. Such variance can be verified with other software or magnetic codes.

8.2 Future Work

DNBPS is a complex system comprising of various subsystems distantly located. In order to assess the fault energy and the corresponding role of the snubbers, a detailed circuit model of the DNBPS system need to be studied including effect of various stray capacitances. Future works shall concentrate on refining the circuit model mainly the saturable core element for snubber effectiveness.

Experimental attempts shall be made to understand the behaviour of snubber under DC biasing and optimizing the B-window for effective utilisation under fault current peaking upto 500A.

References

[1] Alex Van den Bossche and Vencislav Cekov Valchev. Inductors and transformers for power electronics. *CRC press*, (Chaper 3):110–111.

[2] On going works on Snubber design at ITER INDIA.

[3] J.K. Watson. Using parallel complex permeability for ferrite characterization. *IEEE Trans. on Magnetics 25 (1989)*, (5):4224–4226.

[4] Alex Van den Bossche and Vencislav Cekov Valchev. Inductors and transformers for power electronics. *CRC press*, (Chaper 1):14–16.

[5] Hitachi *Metglas*®. `http://www.hilltech.com/pdf/hl-fm10-cFinemetIntro.pdf/`.

[6] On going works on DNBPS TL design at ITER INDIA.

[7] "Calculation of The Effective Parameters of Magnetic Piece Parts". *International Electrotechnical Commission,IEC 60205*, 2001.

[8] Loc Vu-Quoc Paiboon Nakmahachalasint, Khai D.T.Ngo. Effective parameter for toroidal cores based on nonlinear magnetization. *IEEE Trans. on Magnetics, vol. 41, No. 9,September 2005.*

[9] Alberto Pesce. Passive protections against breakdown effects in neutral beam injection devices for nuclear fusion experiments,university of padova. page 85, 2010.

[10] Soft ferrites:A user guide. *Magnetic Materials Producers Association, Chicago, IL*, 1998.

[11] Tutorial on saturable core. `http://www.powersimtech.com/manual/Tutorial%20-%20Saturable%20Core.pdf`.

Index